Water Science & Technology

IWA PUBLISHING

Water Science & Technology Vol 87 No 9, 2061 doi: 10.2166/wst.2023.127

Cr(VI) anion-imprinted polymer synthesized on mesoporous silicon via synergistic action of bifunctional monomers for precise identification and separation of Cr(VI) from aqueous solution by fixed-bed adsorption

Ya Su[a], Yumeng Kang[a], Qinya Huang[a], Jiahao Zhang[a], Jinhua Liu[a], Zhaoyong Hu[b], Zhanchao Liu[b] and Yan Liu[a,*]

[a] School of Chemistry and Chemical Engineering, Jiangsu University, Zhenjiang 212013, China
[b] School of Materials Science and Engineering, Jiangsu University of Science and Technology, Zhenjiang 212003, China
*Corresponding author. E-mail: lyan@ujs.edu.cn

YL, 0000-0003-2026-046X

ABSTRACT

The novel Cr(VI) anion-imprinted polymer (Cr(VI)-IIP) was prepared by a surface imprinting technique with bifunctional monomers pre-assembly system based on mesoporous silicon (SBA-15). The synthesized Cr(VI)-IIP was characterized by Fourier transmission infrared spectra (FT-IR), energy dispersive spectrometer (EDS), scanning electron microscope (SEM), transmission electron microscope (TEM), X-ray powder diffractometer, N_2 adsorption–desorption and thermogravimetric analysis (TGA), proving to be with a highly ordered mesoporous structure, as well as favorable thermal stability. The saturated adsorption amount was 96.32 mg/g, which was 2.7 times higher than that of non-imprinted polymer (NIP). Kinetic experiments showed that the adsorption equilibrium state was obtained within 70 min. In addition, in the selectivity experiments, Cr(VI)-IIP exhibited strong specific recognition ability for Cr(VI) and could realize the separation of Cr(VI) and Cr(III) from an aqueous solution. The dynamic adsorption experiments exhibited that the dynamic adsorption efficiency of Cr(VI)-IIP was as high as 71.57%. Meanwhile, the dynamic regeneration experiments showed that the adsorption amount of Cr(VI)-IIP did not decrease significantly after repeating for five times. All of the findings suggested that Cr(VI)-IIP could achieve precise identification as well as efficient separation of Cr(VI) from aqueous solution.

Key words: adsorption, Cr(VI) and Cr(III), Cr(VI) anion-imprinted polymer, bifunctional monomers, separation

HIGHLIGHTS

- Preparation of Cr(VI) anion-imprinted polymer (Cr(VI)-IIP) by bifunctional monomers pre-assembly system.
- The Cr(VI) imprinted sites formed by the coordination of bifunctional monomers and template ions could realize the separation of Cr(VI) and Cr(III).
- Cr(VI)-IIP exhibited superior selectivity compared to other common adsorbents and Cr(VI) imprinted polymers prepared by a single functional monomer.

GRAPHICAL ABSTRACT

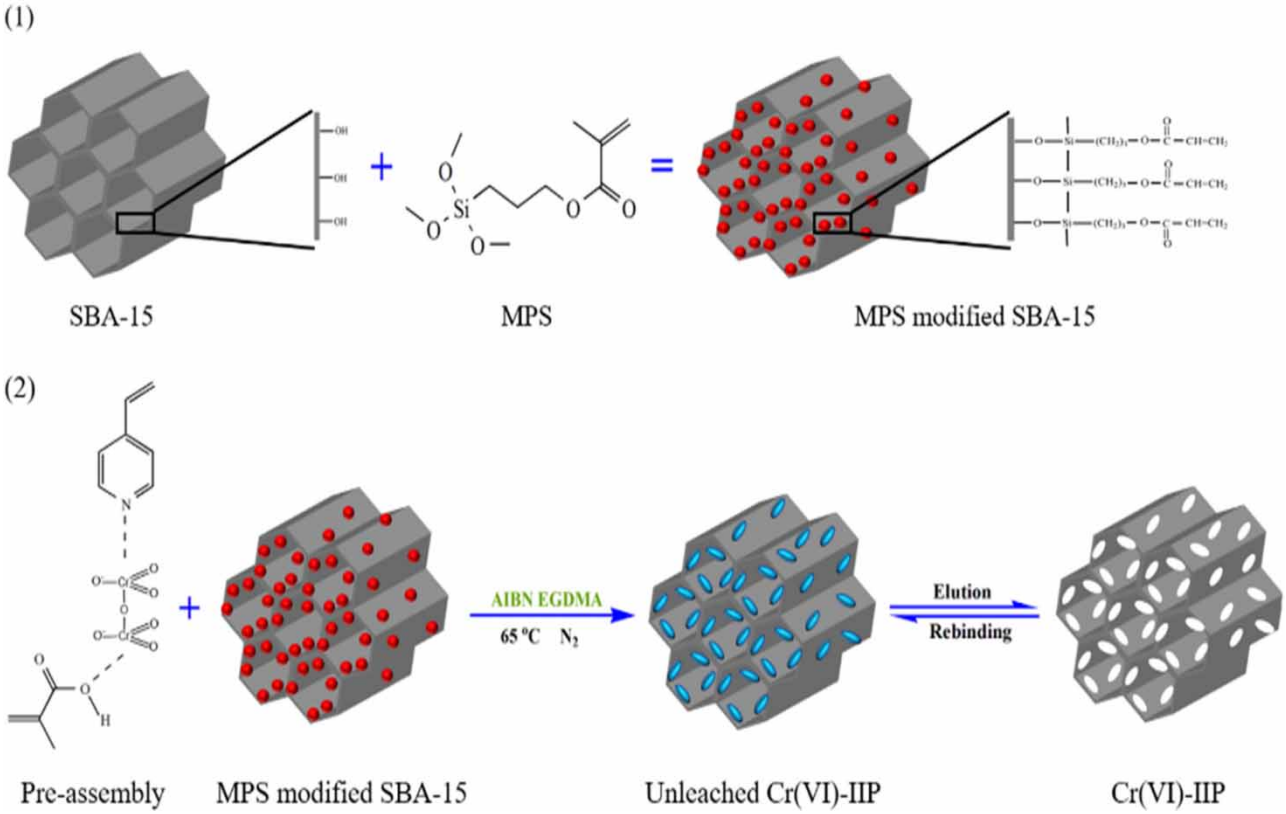

INTRODUCTION

In the process of industrial production such as electroplating, metallurgy, leather making, metal processing and wood preservative, large quantities of wastewater containing Cr(VI) are generated and discharged into the ecological environment, becoming one of the most common pollutants in soil, groundwater and surface water (Kong *et al.* 2021). Chromium in water mainly exists in the forms of Cr(VI) and Cr(III). The toxicity of chromium is related to the valence state, and compounds with different valence states can be converted into each other (Li *et al.* 2023b). Cr(III) is an important micronutrient in the human body, with stable properties and easy-to-produce hydroxide precipitation, which is 100 times less toxic than Cr(VI) (Zhou *et al.* 2020). Different from Cr(III), Cr(VI) has strong mobility and toxicity (Fang *et al.* 2021), which can lead to cell cancerization and even to the death of living organisms (Zhang *et al.* 2019). Therefore, the content of Cr(VI) is an important indicator of water pollution control. The maximum levels of Cr(VI) in drinking water and industrial effluent are regulated by the US Environmental Protection Agency (EPA) within 50 and 200 μg/L, respectively (Jasim *et al.* 2023). As a result, precise detection of Cr(VI) presence in ambient water is critical.

The most commonly used determination methods of chromium are Raman scattering spectroscopy (Wang *et al.* 2022), X-ray fluorescence spectrometry (Ferreira *et al.* 2023), inductively coupled plasma mass spectrometry (ICP-MS) (Pluhacek *et al.* 2023) and atomic absorption spectrometry (AAS) (Rajaram *et al.* 2023). However, these techniques can only measure the total content of Cr, which means the amount of Cr(VI) cannot be detected accurately in water. The interference of Cr(III) should be avoided in order to identify the amount of Cr(VI). Therefore, it is essential to preconcentrate and separate Cr(VI). Undoubtedly, one of the most popular and efficient separation techniques is solid phase extraction (SPE) (Yaida *et al.* 2023). However, general SPE sorbents, such as nano-MnO_2 (Li *et al.* 2023a), ceria decorated titanate nanotubes (Biswas *et al.* 2023), polyethyleneimine (Bagdat *et al.* 2023) and Fe_3O_4@SiO_2@DPC (Assi *et al.* 2019) have poor selectivity. In addition, SPE sorbents for Cr(VI) such as Mil-100 (Fe) (Li *et al.* 2022), Fe-Zn@BC (Zheng *et al.* 2022), water-based magnetic fluid-spores (WMFSs) (Ren *et al.* 2022) and Cit-nZVI@BC (Zhou *et al.* 2022) have the problem of low adsorption capacity. Therefore, it is necessary to develop a preconcentration and separation method for Cr(VI) with high selectivity and adsorption capacity.

Ion-imprinted polymer (IIP) is a synthetic polymer with the function of target ion recognition (Islam & Rais 2023). Due to its unique predetermined recognition performance and applicability, IIP has been widely used in the field of SPE (Giove *et al.* 2023). Some research teams have developed different kinds of IIPs to separate metal ions with different valence states, such as Mo(IV)/Mo(VI) (Fallah & Taghizadeh 2020), As(III)/As(V) (Chen *et al.* 2020), Sb(V)/Sb(III) (Wang *et al.* 2020), and so on. However, these IIPs only use single functional monomers during the pre-assembled phase. Imprinted cavities formed by coordination between a single functional monomer and template ions cannot recognize target ions accurately, and the imprinted cavities have a low affinity for target ions, resulting in unsatisfactory selectivity of IIP (Bao *et al.* 2023). Especially for the separation of different valence states of the same metal elements, due to their close mass, size, coordination number and spatial configuration (Hassanzadeh *et al.* 2018), the imprinted cavity formed by a single functional monomer cannot identify the target ions accurately. In addition, different valence states of the same metal element exist in different forms in solution. For example, Cr(III) generally exists in solution as a cation, while Cr(VI) generally exists as an anion. Most of the traditional IIPs focused on the selective separation of metal cations, but there are few reports dedicated to the preparation of metal anionic imprinted polymers. IIPs for specific anions will achieve more precise identification of the target ions in valence state, spatial configuration and size. At present, the separation of Cr(VI) anion by a single functional monomer is usually poor in selectivity. Therefore, it is important to develop new forms of interaction between functional monomers and template ions to prepare novel metal anionic imprinted polymers, so as to improve and enhance the selectivity of traditional IIPs.

In recent years, some researchers have developed a novel interaction relationship between functional monomers and template molecules to further improve the identification accuracy of IIP, which was constructed by the synergistic action of bifunctional monomers. A batch of new IIPs was synthesized using 4-vinylpyridine (4-VP)/ethylene glycol dimethacrylate (EGDMA) (Nchoe *et al.* 2020) and glycidyl methacrylate (GMA)/acrylamide (AM) (Luo *et al.* 2020), etc., as bifunctional monomers for the separation of Cr(VI) anion. Selectivity studies showed that in the presence of competitive ions, IIP synthesized by bifunctional monomers had a higher selective adsorption capacity for Cr(VI) anion, which was improved significantly compared with traditional IIP prepared by a single functional monomer. However, these IIPs prepared by traditional emulsion, suspension or bulk polymerization will still face problems such as elution difficulty, the poor affinity of the binding site and large mass transfer resistance due to template ion embedding. Therefore, introducing surface imprinting technology based on SBA-15 is an effective method to solve these problems (Xu *et al.* 2021a).

SBA-15 consists of parallel cylindrical pores with axes arranged in a hexagonal unit cell. The regular structure prevents changes in the shape of imprinted sites in the organic polymer (Dobrzyńska *et al.* 2021). The ordered mesoporous structure endows it with a large specific surface area and pore volume. At the same time, it also has the characteristics of a controllable aperture, thick hole wall and good hydrothermal stability (Zhang *et al.* 2023). The large aperture of SBA-15 is conducive to the distribution of imprinted sites in the channel and Cr(VI) transport (Hashami *et al.* 2022). The IIP prepared by a surface imprinting technique based on the unique structural features of SBA-15 not only boosts the adsorption capacity of Cr(VI) but also achieves an excellent dynamic adsorption effect.

In this study, a new type of Cr(VI)-IIP was synthesized on the surface of mesoporous silicon-based material SBA-15 by using surface imprinting technology and a bifunctional monomer pre-assembly system to enhance the adsorption capacity and selective separation capability of Cr(VI) anion. In which, methacrylic acid (MAA) and 4-VP were used as functional monomers and $Cr_2O_7^{2-}$ was selected as the template ion. The separation of Cr(VI) and Cr(III) in an aqueous solution can be better achieved due to the specific recognition and binding affinity of the imprinted sites for $Cr_2O_7^{2-}$. The effects of a series of experimental conditions, such as pH, initial Cr(VI) concentration, temperature and adsorption time on adsorption were investigated in static adsorption experiments, and the mechanism in the adsorption process was studied by adsorption isotherm model and adsorption kinetic model. Since the static adsorption experiments focus on theoretical research and the dynamic adsorption experiments were more focused on practical applications, the dynamic adsorption capacity and dynamic regeneration capacity of Cr(VI)-IIP were investigated in fixed-bed experiments and excellent practical applications were confirmed.

EXPERIMENTAL

Chemicals and instruments

Mesoporous silicon (SBA-15) was synthesized according to the procedure described by Zhao *et al.* (1998), methacrylic acid (MAA), 4-vinylpyridine (4-VP), EGDMA and 2,2′-azobis-isobutyronitrile (AIBN) were purchased from Aladdin Reagent Co.

Ltd (China). Potassium dichromate ($K_2Cr_2O_7$), nickel nitrate hexahydrate ($Ni(NO_3)_2{\cdot}6H_2O$), copper nitrate trihydrate ($Cu(NO_3)_2{\cdot}3H_2O$), cadmium nitrate ($Cd(NO_3)_2{\cdot}4H_2O$), chromium trichloride ($CrCl_3$), sodium hydroxide (NaOH), hydrochloric acid (HCl), methanol (CH_3OH), hexamethylenetetramine (HMA), 1,5-diphenylcarbonyl dihydrazine and 3-methylacryloxypropyl trimethoxysilane (MPS) were purchased from Sinopharm Holding Co. Ltd (China). All reagents used in the experiment were analytical grade and doubly distilled water (DDW) used throughout the experiments was obtained by the laboratory purification system.

TAS-986 flame atomic adsorption spectrometer (FAAS) (Purkinje General, China) and inductively coupled plasma atomic emission spectrometer (ICP-AES) (Varian, USA) were combined to measure the concentrations of Cr(VI) and other mental ions such as Cr(III), Cu(II), Cd(II) and Ni(II). Fourier transmission infrared spectra (FT-IR, 4,000–400 cm^{-1}) in KBr were recorded on a NICOLET NEXUS 4700 FT-IR apparatus (Nicolet, USA). A NOVA2000-specific surface and porosity analyzer (Quntachrome, USA) was used to measure the surface area and pore size distribution. Low-angle X-ray powder diffractometer (XRD) measurements were carried out with a Bruker D8 diffractometer (Bruker, Germany) using an angle of 0.5–8.0° with 1°/min. The morphologies of SBA-15 and Cr(VI)-IIP were observed by a JSM-6480 scanning electron microscope (SEM) (JEOL, Japan) and a JEM-2010 transmission electron microscope (TEM) (JEOL, Japan). Thermogravimetric analysis (TGA) was carried out using a differential scanning calorimeter/differential analysis (DSC/DTA-TG) (STA 449C Jupiter Nexe, Germany). A pHS-3C precision pH meter (Lida, China) was used for the pH value adjustments.

Preparation of MPS-modified SBA-15

First, SBA-15 was dispersed into 3 mol/L HCl for reflux for 24 h. After activation, the activated SBA-15 was washed with DDW until to neutral and dried. Next, the 0.1 g dried SBA-15 was dispersed into 40 mL ethanol solution with ultrasonic dispersion. Then, the mixture of 2.5 mL MPS and 10 mL ethanol was added slowly into the solution under the condition of 50 °C water bath heating and magnetic stirring and reacted for 12 h. The product was centrifuged and cleaned with ethanol to remove unreacted coupling agents. Finally, MPS-modified SBA-15 was dried under vacuum at 50 °C for 12 h.

Preparation of Cr(VI)-IIP and NIP

In a 100 mL three-necked flask, 73.5 mg $K_2Cr_2O_7$ (0.5 mmol Cr(VI)), 86 μL MAA (1 mmol) and 108 μL 4-VP (1 mmol) were added into 40 mL mixed solutions (CH_3OH/DDW, v/v 3:1) and reacted for 2 h with magnetic stirring. Then, the pre-assembly solution was purged with N_2 and then 10 mg AIBN, 10 mL EGDMA and 0.1 g MPS-modified SBA-15 were dispersed into this suspension. Afterwards, under N_2 protection, the mixture was refluxed at 65 °C and stirred for 6 h. After polymerization, the polymer was cooled with an ice-water bath and collected by suction filtration with a Buchner funnel. To remove the residual monomers, the polymer was washed with CH_3OH/DDW (1:1, v/v) for three times. Then, the chelated Cr(VI) in the polymer was eluted with 2 mol/L HCl under magnetic stirring. ICP-AES was applied to determine the Cr content (Kachbi *et al.* 2022). The eluate was detected by ICP-AES until no template ion $Cr_2O_7^{2-}$ left in the eluate to ensure that Cr(VI) was eluted completely in the polymer. Finally, the polymer was washed with DDW until neutral and dried under vacuum at 60 °C for 24 h. As a comparison, the NIP was synthesized under the same conditions without $K_2Cr_2O_7$.

Static adsorption experiments

The static binding behaviors of Cr(VI)-IIP and NIP for Cr(VI) under different experimental conditions were investigated in batch adsorption experiments. The accurate amount of Cr(VI) in the solution was detected by ICP-AES. The detailed experimental procedure and calculation equations were shown in Supplementary Data.

Selective adsorption experiment

The selective recognition ability of Cr(VI) by Cr(VI)-IIP and NIP was evaluated by adsorption tests in binary solutions containing Cr(VI) and interfering ions M such as Cr(III), Cu(II), Cd(II) and Ni(II). The selective adsorption experiments were studied with 10 mg/L of each metal ion and 10 mg Cr(VI)-IIP or NIP in 25 mL colorimetric tube under room temperature. In particular, diphenylcarbazide spectrophotometric method combined with ICP-AES detection technology was used to detect Cr(VI) and Cr(III) (Alahmad *et al.* 2019). First, the concentration of total Cr was measured by ICP-AES, and then diphenylcarbazide and Cr(VI) formed a stable purple-red chrome compound, and its absorbance was measured at the maximum absorption wavelength of 550 nm with a spectrophotometer, thereby obtaining Cr(VI) concentration (Mohana Rangan *et al.* 2021). Finally, the concentration of Cr(III) was thus obtained by subtraction of Cr(VI) concentration from the total

concentration of Cr (Liu *et al.* 2013). Other ion concentrations were detected by ICP-AES. The relevant calculation formulas were given in Supplementary Data.

Dynamic adsorption and regeneration experiments

0.1 g of adsorbent (Cr(VI)-IIP/NIP) was added into a self-made dynamic column with a diameter of 1.0 cm and a length of 15 cm. The concentration of Cr(VI) in the inflow solution was 10 mg/L, and the flow rate was controlled at 1 mL/min. The outflow solution was collected every 5 min, and the content of Cr(VI) in the outflow solution was detected via ICP-AES. When the fixed bed reached the adsorption equilibrium, the saturated Cr(VI)-IIP was eluted continuously with 2 mol/L HCl at a flow rate of 1 mL/min until Cr(VI) was not detectable in the eluate. Then, the Cr(VI)-IIP was washed to neutral with copious amounts of DDW and continued for the next fixed-bed cycle. The dynamic adsorption capacity q_e, the total adsorption capacity q_{total}, the volume of solution flowing through the fixed bed at adsorption equilibrium V_e (L), empty bed contact time (EBCT) and the separation efficiency (Y%) were given in Supplementary Data.

Sample preparation and analysis

To verify the accuracy and applicability of the experimental method, river water samples from the Yudai River (Zhenjiang, China) and tap water from our laboratory were selected for analysis. All samples were filtered off suspended particles through a 0.45 μm Millipore membrane, then acidified with nitric acid (pH of water samples adjusted to 2) and stored at 4 °C in darkness. After that, the concentrations of Cr(VI) in water samples and the recovery rate of Cr(VI)-IIP to Cr(VI) were analyzed by the standard addition method.

RESULTS AND DISCUSSION

Characterization of the materials

FT-IR spectra of SBA-15(a), MPS-modified SBA-15(b) and Cr(VI)-IIP(c) were illustrated in Figure 1. As presented in Figure 1, the spectra of SBA-15 in Figure 1(a) and MPS-modified SBA-15 in Figure 1(b) had a strong characteristic peak at 1,080 cm^{-1} and two relatively weak peaks at 806 and 461 cm^{-1}, which were attributed to the stretching and bending vibrations of Si–O–Si, indicated that the structure of SBA-15 did not change after the modification by MPS (An *et al.* 2022). However, these three characteristic peaks in the infrared spectrum of Cr(VI)-IIP in Figure 1(c) were shifted in the long wavelength direction to 1,139, 825 and 464 cm^{-1}, respectively. The presence of these three peaks was attributed to the Si–O–Si backbone structure did not change. At the same time, the shift of the three peaks was attributed to the length of Si–O–Si bond was changed during the polymerization process (Wang *et al.* 2012; Ellerbrock *et al.* 2022). Besides, the peak at 1,636 cm^{-1} for Si-OH of SBA-15 still can be observed in all spectra. The above results indicated that the silicon-based material SBA-15 was well preserved in

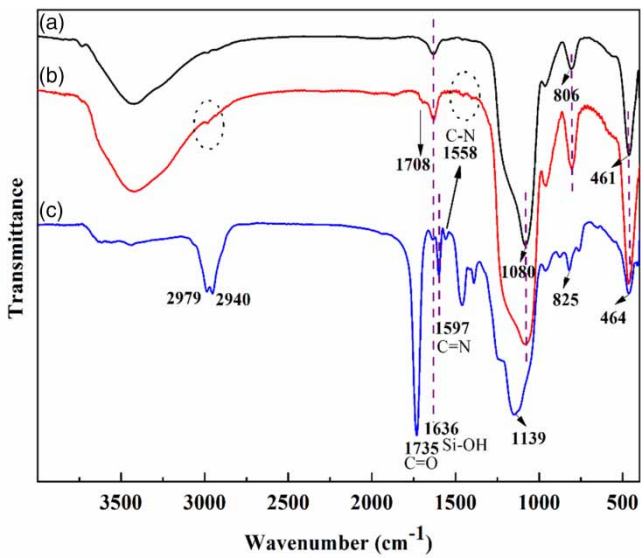

Figure 1 | FT-IR spectra of (a) SBA-15, (b) MPS-modified SBA-15 and (c) Cr(VI)-IIP.

MPS-modified SBA-15 and Cr(VI)-IIP. However, when compared with SBA-15 in Figure 1(a), two new peaks appeared at 1,708 and 2,940 cm^{-1} in MPS-modified SBA-15 in Figure 1(b), which were caused by the stretching of C = O and C–H bonds on MPS, respectively, indicated that SBA-15 was modified by MPS successfully (An *et al.* 2022). In addition, compared with MPS-modified SBA-15 in Figure 1(b), two new peaks appeared at 1,597 and 1,558 cm^{-1} in Cr(VI)-IIP in Figure 1(c), which were caused by stretching of C = N and C–N bonds on 4-VP (Meng *et al.* 2014), respectively. Moreover, the peak at 1,708 cm^{-1} for C = O bond in Cr(VI)-IIP in Figure 1(c) was shifted to 1,735 cm^{-1} and the peak of the C–H bond became stronger at 2,979 cm^{-1}, which were due to the coordination of the MAA monomer with the target ions during the imprinted polymerization (Liu *et al.* 2017). In conclusion, Cr(VI)-IIP was prepared successfully.

The elemental composition of the imprinted polymer was analyzed by EDS. The EDS spectra of (a) before the adsorption of Cr(VI)-IIP and (b) after the adsorption of Cr(VI)-IIP were shown in Figure 2. It could be clearly seen that the signals of C, N, O and Si elements were detected in the spectrum before the adsorption of Cr(VI)-IIP in Figure 2(a), but no signal of Cr element, indicated that the template ions in the imprinted polymer had been eluted completely. However, when compared with the spectrum before the adsorption of Cr(VI)-IIP in Figure 2(a), the signal of Cr element was also detected in the spectrum after the adsorption of Cr(VI)-IIP in Figure 2(b) in addition to the signals of C, N, O and Si elements, indicating that Cr(VI) was adsorbed on Cr(VI)-IIP successfully.

The SEM images of SBA-15 and Cr(VI)-IIP were presented in Figure 3(a) and 3(b), respectively. As presented in Figure 3(a), the SBA-15 was constituted of a number of short rods with a regular shape of about 1 μm. However, in Figure 3(b), the ordered structural characteristic of SBA-15 was destroyed slightly, and the surface became rough, which were due to a series of functionalization and the formation of polymers on its surface. The TEM images of the two samples were presented in Figure 3(c) and 3(d), respectively. The ordered mesoporous channel structure can be observed clearly in the substrate SBA-15 (Xu *et al.* 2021). As for Cr(VI)-IIP, the mesoporous channel became narrow and fuzzy due to the loaded of polymer on the surface of the substrate, but the original order of the mesoporous structure was still maintained to a certain extent.

The low-angle XRD curves of SBA-15 and Cr(VI)-IIP were exhibited in Figure 4. Obviously, in the range of 0.5°–5°, the matrix material had a strong diffraction peak at 0.8, which corresponded to the diffraction peak of the (100) reflection of typical SBA-15. In addition, the two smaller diffraction peaks near 1.5° and 1.7° corresponded to the diffraction peaks of (110) and (200) of SBA-15, respectively. These indicated that the prepared matrix material had a typical two-dimensional hexagonal mesoporous structure (Sobrinho *et al.* 2019). However, the diffraction peaks of Cr(VI)-IIP on (100), (110) and (200) reflections were shifted, respectively, and the intensity of diffraction peaks on (100) reflection was weakened obviously, indicating that the polymer layer was formed not only on the surface of SBA-15 but also in the mesoporous channel during the imprinting process (Perez-Quintanilla *et al.* 2007). However, three typical Bragg diffraction peaks still existed

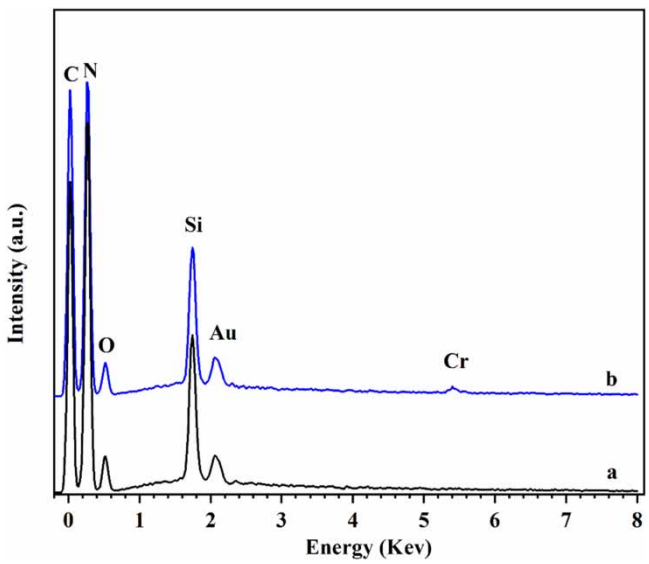

Figure 2 | EDS spectra of (a) before the adsorption of Cr(VI)-IIP and (b) after the adsorption of Cr(VI)-IIP.

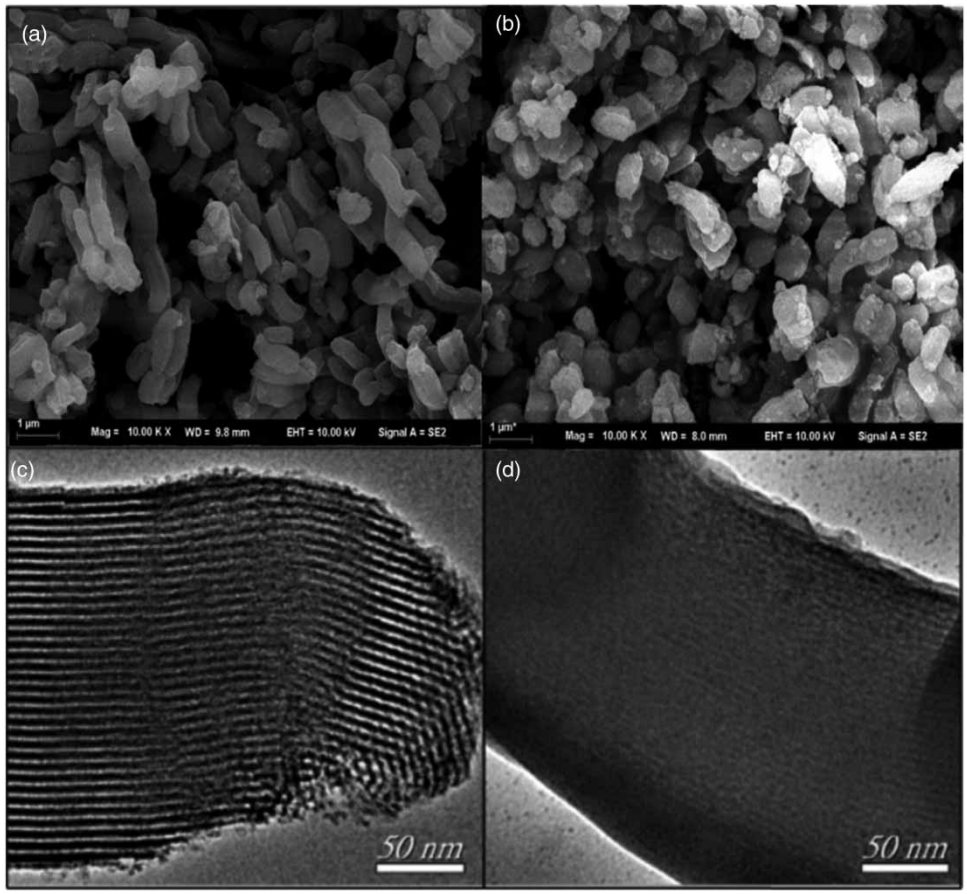

Figure 3 | SEM images of (a) SBA-15 and (b) Cr(VI)-IIP, TEM images of (c) SBA-15 and (d) Cr(VI)-IIP.

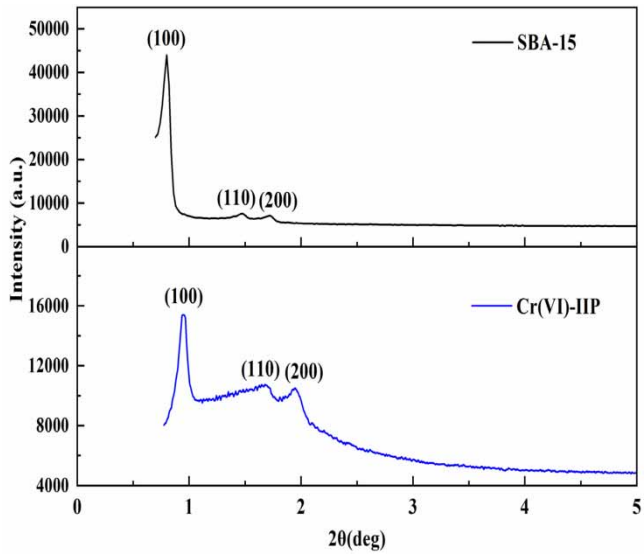

Figure 4 | The low-angle XRD patterns of SBA-15 and Cr(VI)-IIP.

in Cr(VI)-IIP, indicating that Cr(VI)-IIP retained the two-dimensional hexagonal crystal structure of the original SBA-15 after polymerization.

The results of N_2 adsorption–desorption isotherms on the mesoporous carriers SBA-15 and Cr(VI)-IIP were presented in Figure 5. The curves obtained from the two samples belong to Langmuir type IV isotherm with an H1 hysteresis loop. According to the IUPAC definition, these were the main characteristics of a typical mesoporous structure, indicating that the synthesized IIP still maintained the mesoporous structure of SBA-15 (Moritz & Laniecki 2012). Moreover, it could be clearly seen from the inset of Figure 5 that Cr(VI)-IIP still maintained the similar pore size distribution of SBA-15, which further indicated that Cr(VI)-IIP had a regular mesoporous channel structure. According to the data, the specific surface area, pore size and pore volume of SBA-15 were 642.23 m^2/g, 4.4 nm and 0.72 cm^3/g, respectively, while these parameters of Cr(VI)-IIP were 374.15 m^2/g, 3.8 nm and 0.58 cm^3/g, respectively. These parameters of Cr(VI)-IIP decreased significantly. These were due to the fact that the polymer formed by 4-VP and MAA was immobilized on the outer surface of mesoporous material and the inner wall of the channel during the imprinting polymerization. Thanks to the large specific surface area provided by the mesoporous material SBA-15, the Cr(VI)-IIP had a large number of imprinted sites (Zeng *et al.* 2021). In addition, Cr(VI)-IIP with ordered mesoporous structure was favorable for Cr(VI) transport, thereby leading to enhanced adsorption kinetic (Sun *et al.* 2018).

To study the thermal stability of SBA-15 and Cr(VI)-IIP, as well as the mass fraction of the polymer supported on the substrate surface, the samples were subjected to TGA at a heating rate of 10 °C/min under N_2 protection. As presented in Figure 6, only a 5.16% mass loss of SBA-15 in the process of rising from room temperature to 200 °C was observed, and the mass remained basically unchanged after that, which was mainly caused by evaporation of water adsorbed on SBA-15. The TGA curve of Cr(VI)-IIP presented two declining stages: 6.18% mass loss before 200 °C was caused by evaporation of water adsorbed by the physical sample; the mass loss of 14.67% from 250 to 500 °C was caused by thermal decomposition of the imprinted polymer layer on SBA-15. In addition, the mass fraction of the polymer was only 14.67%, indicating that the imprinted polymer layer on SBA-15 was thin.

Adsorption studies

At room temperature, the influence of pH changes (1–8) on the adsorption process was investigated in the solution with the initial Cr(VI) concentration of 10 mg/L. The relationship between the adsorption capacity of Cr(VI)-IIP and NIP with the change of solution pH were shown in Figure 7(a). As given in Equation (1), in pH = 1, H_2CrO_4 was the main form of Cr(VI). Due to the existence of $Cr_2O_7^{2-}$ imprinted sites in Cr(VI)-IIP, the imprinted sites were not selective for H_2CrO_4. However, the adsorption properties of nitrogen atoms (from 4-VP) and oxygen atoms (from MAA) on Cr(VI)-IIP and NIP also changed with the change of pH. When the pH was low, the protonation phenomenon was obvious and the combination

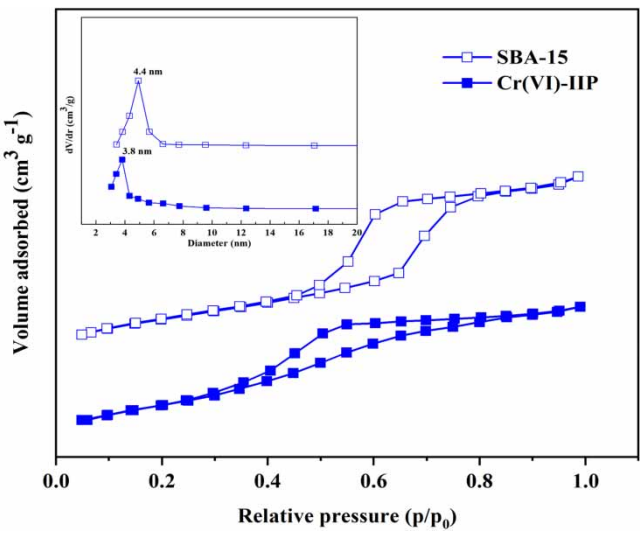

Figure 5 | N_2 adsorption–desorption isotherms and Barret-Joyner-Halenda (BJH) pore size distribution (inset) of SBA-15 and Cr(VI)-IIP.

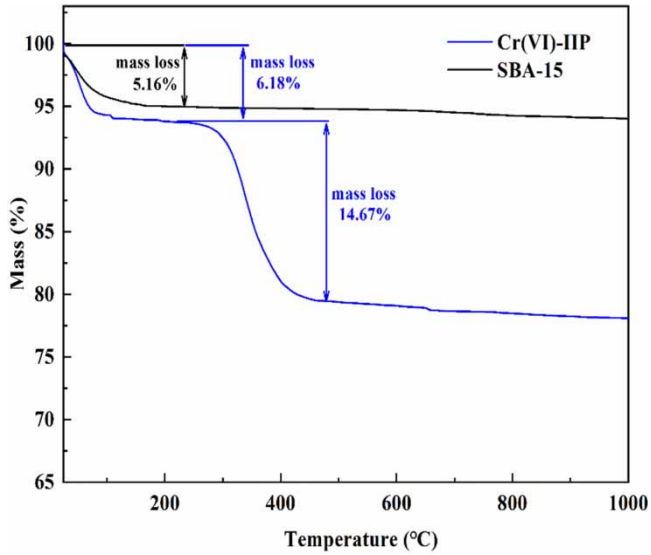

Figure 6 | Thermogravimetric analysis of SBA-15 and Cr(VI)-IIP.

of functional groups and H^+ would enhance the adsorption of Cr(VI) anion by the adsorbents (Deng & Bai 2004). While the solutions pH were between 2 and 6, Cr(VI) was found in the form of $HCrO_4^-$ and $Cr_2O_7^{2-}$ and the reaction process was shown in Equation (2). At this point, the imprinted sites began to adsorb $Cr_2O_7^{2-}$. However, with the increase of pH, the protonation of functional groups weakened and the ability of adsorbing Cr(VI) anion decreased. At the same time, with the increase of OH^- concentration, there was a competitive adsorption phenomenon between OH^- and Cr(VI) anion, the ability of functional groups captured target ion was also reduced. When the pH increased from 6 to 8, Cr(VI) was only found as CrO_4^{2-} and the reaction process was shown in Equation (3) (Benhammou *et al.* 2007), the adsorption of Cr(VI) by the two absorbents was unfavorable. The results showed that both absorbents exhibited higher adsorption capacity at pH = 2. To sum up, the pH = 2 was selected as the condition for a series of subsequent adsorption experiments. In the solutions of different pH, the change processes of Cr(VI) forms were as follows:

$$H_2CrO_4 \leftrightarrow HCrO_4^- + H^+ \tag{1}$$

$$Cr_2O_7^{2-} + H_2O \leftrightarrow 2HCrO_4^- \tag{2}$$

$$HCrO_4^- \leftrightarrow CrO_4^{2-} + H^+ \tag{3}$$

The influence of C_0 (initial concentration of Cr(VI)) on adsorption performance of adsorbents was investigated at room temperature. As presented in Figure 7(b), the adsorption capacities of the two adsorbents increased sharply at lower C_0, and then the adsorption capacities reached saturation and remained constant after reaching a certain concentration. For Cr(VI)-IIP, when C_0 reached 200 mg/L, the adsorption amount of Cr(VI)-IIP reached saturation, and its saturation adsorption amount was 96.32 mg/g. For NIP, when C_0 exceeded 100 mg/L, the adsorption amount of NIP reached saturation, and its saturation adsorption amount was 35.68 mg/g. The saturation adsorption amount of Cr(VI)-IIP was about 2.7 times more than that of NIP. This was mainly because the functional monomers 4-VP and MAA constituted a large number of Cr(VI) imprinted sites after coordination with template ions, which had strong specific recognition ability for Cr(VI). By comparison, there were no imprinted sites on NIP, and the NIP only had a simple electrostatic interaction with Cr(VI), so the adsorption amount was limited.

The temperature had a significant impact on the adsorption of Cr(VI). The adsorption capacities of the two adsorbents at different temperatures were investigated. As presented in Figure 7(c), both absorbents showed the best adsorption performance for Cr(VI) at 25 °C, and the adsorption capacities decreased gradually as temperature increased. This phenomenon

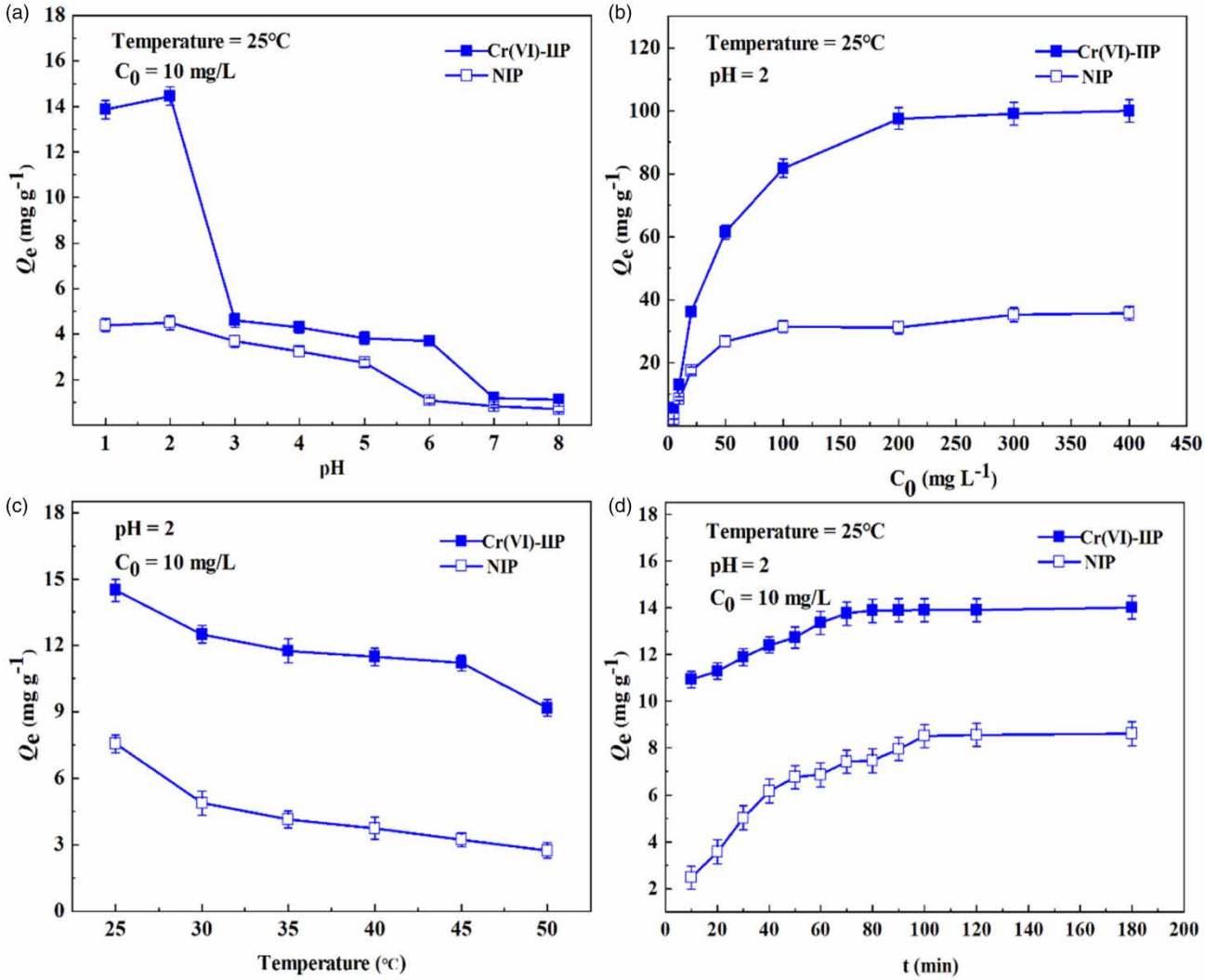

Figure 7 | Influence of the static adsorption experiment conditions ((a) pH of solution, (b) initial Cr(VI) concentration of solution, (c) temperature, (d) adsorption time).

might be due to the adsorption processes of adsorbents being exothermic, and the low temperature was conducive to adsorption. Therefore, the temperature of 25 °C was selected as the condition for a series of subsequent experiments.

Adsorption isotherms

The adsorption isotherms described the distribution of adsorbed substances in the adsorbents and solution when the solid-liquid two phases reach equilibrium at a specific temperature and different concentrations. Therefore, the Langmuir (Dolai *et al.* 2019), Freundlich (Abu-Alsoud *et al.* 2020) and Temkin (Zeng *et al.* 2022) adsorption isotherm models were introduced to fit and analyze the adsorption behaviors of the two absorbents, and the results of the nonlinear fits were shown in Figure 8. First, the adsorption capacity of Cr(VI)-IIP increased rapidly with increasing Cr(VI) concentrations because the imprinted sites on Cr(VI)-IIP were sufficient to adsorb Cr(VI). However, when the Cr(VI) concentration increased gradually and arrived at a certain value, due to the high concentration of Cr(VI) competing fiercely for the limited surface active sites on Cr(VI)-IIP, resulting in a slow increase of Cr(VI)-IIP adsorption amount and finally reached saturation state. The adsorption process of NIP followed the same trend as that of Cr(VI)-IIP, but due to the lack of imprinted sites on NIP, NIP reached the saturation state at a smaller Cr(VI) concentration. The saturation adsorption amount of Cr(VI)-IIP was 96.32 mg/g, while that of NIP was only 35.68 mg/g. The computational procedure of Langmuir, Freundlich and Temkin

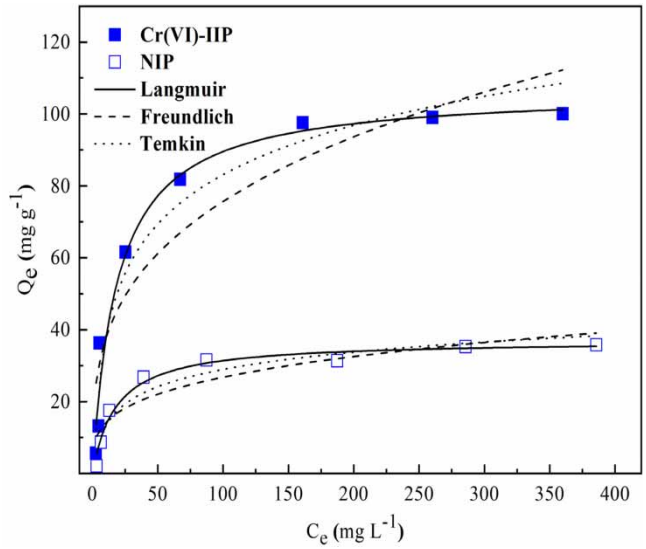

Figure 8 | Adsorption isotherm models of Cr(VI) adsorption onto Cr(VI)-IIP and NIP.

models were shown in Supplementary Data, and the relevant parameters obtained from the calculations were shown in Supplementary Table S1. According to the data in Table S1, the theoretical saturation adsorption amounts of Cr(VI)-IIP and NIP calculated by the Langmuir equation were 106.55 and 37.02 mg/g, respectively, which were close to the experimental data (96.32 and 35.68 mg/g). The dimensionless values R_L ranged from 0 to 1, which confirmed that the adsorption processes of the two absorbents were favorable adsorption. Moreover, the values of $1/n$ calculated by the Freundlich nonlinear regression equation also ranged from 0 to 1, which also demonstrated that the adsorption processes of the two absorbents were advantageous. Variation of Gibbs free energy $\Delta G^0 < 0$ indicated that the adsorption processes of the two absorbents were spontaneous, and the calculated K_T values were between 0 and 1, which proved that during the adsorption processes, as the adsorbents were covered by Cr(VI), the adsorption heat generated by the adsorption decreased gradually. In addition, by comparing the R^2 of the three models, it was concluded that the Langmuir model ($R^2 > 0.96$) was the most suitable to describe the Cr(VI)-IIP and NIP adsorption behaviors, indicating that the adsorption reaction occurred on the surface of the adsorbents.

Adsorption kinetics

Since the adsorption rate was a critical parameter to describe the adsorption kinetics, the adsorption capacities of the adsorbents at different times were investigated. Figure 7(d) showed that the adsorption amounts of both adsorbents increased gradually with the extension of adsorption time, and finally tended to equilibrium state. The adsorption equilibrium time of Cr(VI)-IIP and NIP were 70 and 100 min, respectively. Cr(VI)-IIP reached adsorption equilibrium significantly earlier than NIP, which was not only because of the imprinted sites formed by bifunctional monomers and template ions had strong coordination ability with Cr(VI), but also because of the easy contact of imprinted sites on the mesoporous materials SBA-15 with low mass transfer resistance. Moreover, due to the lack of Cr(VI) imprinted sites on NIP (Li *et al.* 2011), resulted in a lack of binding affinity for Cr(VI), which made the adsorption rate relatively slow.

To further explore the adsorption mechanism during Cr(VI)-IIP adsorption, the adsorption experimental data in Figure 7(d) were analyzed by pseudo-first-order (PFO) kinetic model (Hua *et al.* 2019) and pseudo-second-order (PSO) kinetic model (Lin *et al.* 2020). The PFO and PSO nonlinear curves and the relevant parameters were presented in Figure 9 and Table S2, respectively. The calculation formulas of PFO and PSO were listed in supporting information. By comparing the regression determination coefficient R^2 of PFO and PSO, it was easy to find that the R^2 of PSO for Cr(VI)-IIP was much larger than that of PFO. Moreover, the theoretical Q_e of Cr(VI)-IIP calculated by the PSO rate equation was close to the experimental data ($Q_{e(exp)}$), which demonstrated that Cr(VI)-IIP adsorption conformed to the PSO kinetic model, and the adsorption was chemical adsorption process.

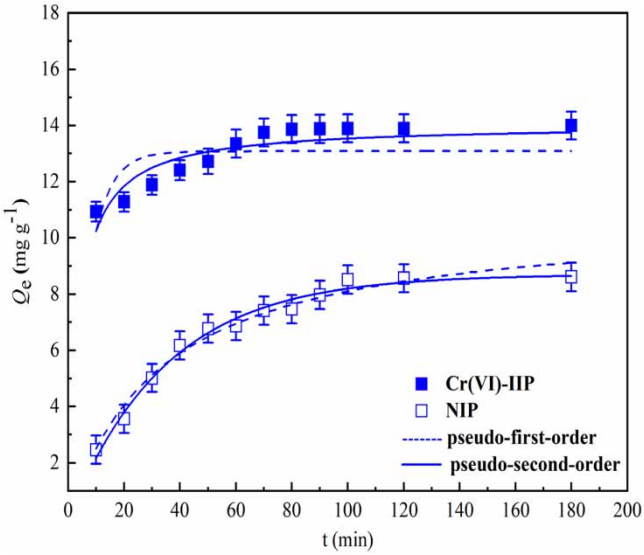

Figure 9 | Adsorption kinetic models of Cr(VI) adsorption onto Cr(VI)-IIP and NIP.

Dynamic adsorption experiment

In the fixed-bed experiments, Cr(VI)-IIP and NIP were filled into the dynamic column, and the dynamic adsorption properties of Cr(VI) by the two adsorbents were investigated. The breakthrough curves of the two adsorbents were performed in Figure 10 and the corresponding parameters were given in Table 1. The curve penetration time t_b and adsorption saturation time t_e of Cr(VI)-IIP lagged behind that of NIP obviously, which resulted in a higher saturation adsorption amount $q_{equation}$ of Cr(VI)-IIP than NIP under the same conditions. According to the calculation, the $q_{equation}$ of Cr(VI)-IIP and NIP were 10.02 and 3.47 mg/g, respectively, which showed that Cr(VI)-IIP still had specific adsorption performance for target ions in the dynamic adsorption experiment. In addition, the $q_{equation}$ of Cr(VI)-IIP and NIP were slightly lower than the equilibrium adsorption capacity Q_e (14.08 and 8.62 mg/g) in the static adsorption experiment, which might be caused by the short contact time between Cr(VI) in solution and adsorbents when it flowed through the fixed bed in the dynamic adsorption experiment. On the whole, the dynamic adsorption behavior of Cr(VI)-IIP was relatively ideal, and the dynamic adsorption efficiency

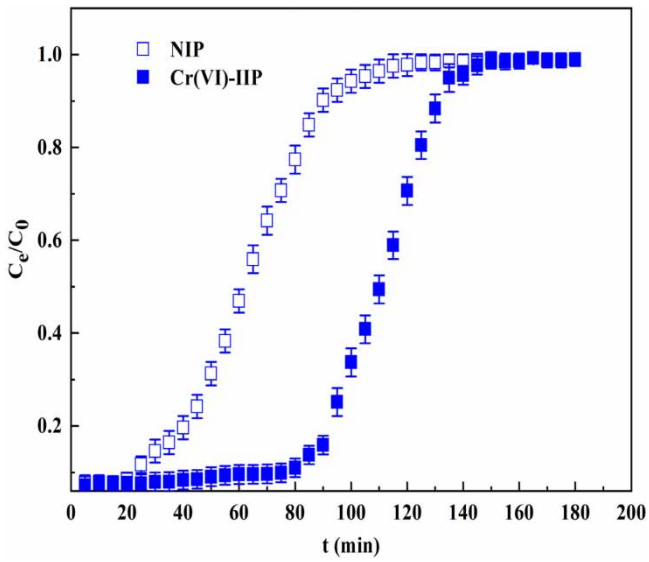

Figure 10 | Dynamic adsorption curves of Cr(VI)-IIP and NIP for Cr(VI).

Table 1 | Parameters in fixed-bed column for Cr(VI) adsorption by Cr(VI)-IIP and NIP

Sorbents	t_b (min)	t_e (min)	q_{total} (mg)	$q_{equation}$ (mg/g)	V_E (L)	Y (%)
Cr(VI)-IIP	80	140	1.00	10.02	140	71.57
NIP	20	105	0.35	3.47	105	33.05

Y was as high as 71.57%, indicating that Cr(VI)-IIP prepared from bifunctional monomer was an ideal SPE adsorbent to treat Cr(VI) in aqueous solution.

Selective adsorption experiment

The specific recognition and binding ability of Cr(VI)-IIP and NIP for Cr(VI) were investigated in binary mixed solutions of Cr(VI)/Cr(III), Cr(VI)/Cu(II), Cr(VI)/Cd(II) and Cr(VI)/Ni(II), respectively. These four metal ions were selected as competing ions for Cr(VI) based on the principle of the same element or the same charge. The experimental results were given in Table 2. The K_d value of Cr(VI) ($K_d = 4{,}351$ mL/g) was much larger than that of Cr(III) ($K_d = 290$ mL/g), illustrating that the prepared Cr(VI)-IIP could realize the separation of different valence states of Cr element. Meanwhile, the K_d of NIP for competing ions was close, leading to the k_{NIP} around 1. In contrast, the k_{IIP} for competing ions was far greater than 1. These data proved that Cr(VI)-IIP had a strong selective adsorption ability for Cr(VI) under the interference of other metal ions. Moreover, according to the values of k', Cr(VI)-IIP had a higher selective adsorption capacity for Cr(VI) than NIP. These were because during the imprinted process, functional monomers 4-VP and MAA were coordinated to Cr(VI) to form abundant Cr(VI) imprinted sites, which had a strong specific recognition ability for Cr(VI) (Fei *et al.* 2021). However, functional monomers in NIP were polymerized randomly, resulting in a random arrangement of functional groups on the polymer surface (Guo *et al.* 2013). These functional groups do not have specific recognition ability for Cr(VI), so the NIP had no selective adsorption ability for Cr(VI).

Dynamic regeneration experiment

The regeneration performance of the adsorbent was very important in fixed-bed experiment. Therefore, the adsorption–desorption experiments of Cr(VI)-IIP were also studied. Under the same adsorption and elution experimental conditions, the adsorbed Cr(VI) was eluted with 2 mol/L HCl, and the adsorption performance of the same batch of adsorbents filled into the dynamic column was studied. The results were shown in Table 3, In the first cycle: during the adsorption process, the t_b and t_e of the Cr(VI)-IIP in the fixed bed were 80 and 140 min, respectively, and the equilibrium adsorption amount was 10.02 mg/g. In the elution process, only 15 mL of 2 mol/L HCl was used to elute the adsorbent, and the elution efficiency was up to 98.2%. With the increase in the number of experimental cycles, it could be found that the penetration time and equilibrium time of the adsorbent in the fixed bed shorten slightly, but after five cycles, the equilibrium adsorption capacity was still up to 9.03 mg/g. In addition, after 20 mL 2 mol/L HCl was eluted, the elution efficiency was still up to 90.0%. The high elution efficiency might be determined by the mesoporous structure of the adsorbent. Large specific surface area and fast mass transfer rate enable the eluent to reach the imprinted sites quickly. Moreover, the eluent of the mobile phase in the fixed bed was more conducive to the elution of the target ion. Overall consideration, the Cr(VI)-IIP had strong regeneration ability and great potential for metal ion separation in fixed-bed experiments.

Table 2 | Distribution coefficient and selectivity coefficient data of Cr(VI)-IIP and NIP

	Cr(VI)-IIP		NIP		
Metal ions	K_d (mL/g)	k_{IIP}	K_d (mL/g)	k_{NIP}	k'
Cr(VI)	4,351		244		
Cr(III)	290	15.00	201	1.21	13.79
Cu(II)	452	9.63	570	0.43	22.40
Cd(II)	261	16.67	271	0.90	18.52
Ni(II)	348	12.50	344	0.71	17.61

Table 3 | Adsorption–desorption parameters for five cycles

Cycle No.	t_b/t_e (min)	Elution volume (mL)	Breakthrough uptake (mg/g)	Desorption amount (mg/g)	Desorption efficiency (%)
Cycle 1	80/140	15	10.02	9.84	98.2
Cycle 2	75/135	20	9.78	9.56	97.7
Cycle 3	75/130	20	9.55	9.16	95.9
Cycle 4	70/125	20	9.12	8.47	92.9
Cycle 5	70/120	20	9.03	8.13	90.0

Sample analysis

The dynamic column filled with Cr(VI)-IIP adsorbent was used to treat the actual water samples from tap water and Yudai River (Zhenjiang, China) successfully. From the experimental results in Table 4, the recoveries of Cr(VI) in the two samples ranged from 97.9 to 104.8%, and the relative standard deviations ranged from 0.1 to 2.3%, indicating that the potential application of the prepared novel Cr(VI)-IIP combined with ICP-AES for the separation and detection of trace metal ions in water samples.

Comparison with other similar type of adsorbents

The adsorption performance of Cr(VI)-IIP prepared in this experiment was compared with that of other Cr(VI) adsorbents, such as equilibrium time, adsorption capacity and selectivity. As shown in Table 5, first, the Cr(VI)-IIP had a great advantage in selectivity compared with other common Cr(VI) adsorbents (Faleschini *et al.* 2023; Li *et al.* 2023c, 2023d; Mao *et al.* 2023), this was attributed to the strong specific recognition ability of Cr(VI) by the imprinted cavity left after the functional monomers chelated with the target ion during the preparation of Cr(VI)-IIP, illustrated that the effectiveness of ion imprinting technique. Afterwards, compared with Cr(VI)-imprinted polymers prepared from single functional monomer such as 4-VP (Nchoe *et al.* 2020), 3-aminopropyltriethoxysilane (APTES) (Zhang *et al.* 2022) and 1-vinylimidazole(1-VI) (Hassanzadeh *et al.* 2018), Cr(VI)-IIP showed a large improvement in adsorption capacity and selectivity. Finally, compared to Cr(VI)-imprinted polymers prepared with bifunctional monomers such as 4-VP/methyl methacrylate (MMA) (Neolaka *et al.* 2018) and 4-VP/2-hydroxyethyl methacrylate (HEMA) (Taghizadeh & Hassanpour 2017), the advantages of Cr(VI)-IIP were mainly reflected in the higher adsorption amount and superior selectivity, though its adsorption equilibrium time was not the shortest. Clearly, the advantage here was the establishment of the synergy between the pre-assembly system of bifunctional monomers and surface imprinting technology based on mesoporous silicon material SBA-15.

CONCLUSION

A novel Cr(VI)-IIP was synthesized on the surface of SBA-15 using MAA and 4-VP as bifunctional monomers and Cr(VI) anion as template ion by surface thermal initiation imprinting technique. A series of static adsorption experiments showed that Cr(VI)-IIP exhibited the best adsorption performance when the solution pH was 2 and the temperature was room temperature, and the saturation adsorption capacity was obviously higher than that of NIP under the same conditions. The

Table 4 | Determination and recoveries of Cr(VI) in samples

Sample	Cr(VI) added (ug/L)	Cr(VI) founded (ug/L)	Recovery ± RSD (%)
Tap water	0	5.28 ± 0.2	
	20	26.13 ± 0.3	104.3 ± 2.3
	50	56.67 ± 0.7	102.8 ± 1.8
	100	103.84 ± 1.4	98.6 ± 1.6
Yudai River water	0	23.12 ± 0.3	
	20	42.69 ± 0.1	97.9 ± 1.8
	50	75.51 ± 0.5	104.8 ± 1.5
	100	123.84 ± 0.6	100.7 ± 0.9

Table 5 | Comparison with other similar type of adsorbents for Cr(VI)

Adsorbents	Equilibrium time (min)	Q_e (mg/g)	Selectivity interferent	$k_{analyte/interferent}$	Reference
Woolen sludge	240	1.1	–	–	Faleschini *et al.* (2023)
Biochar-supported nanoscale zero-valent iron	30	48.45	–	–	Mao *et al.* (2023)
Chitosan-coated magnetic carbon	40	83.4	–	–	Li *et al.* (2023d)
Mg/Al-layered double hydroxides	180	177.88	–	–	Li *et al.* (2023c)
β-cyclodextrin IIP(4-VP)	720	16.9	Cr(III)	1.17	Nchoe *et al.* (2020)
Diatom IIP(APTES)	120	2.5	Al(III) Fe(III)	1.72 1.42	Zhang *et al.* (2022)
Polyacrylonitrile IIP(1-VI)	12	183.62	Cr(III) Cd(II) Cu(II)	3.448 8.409 10.093	Hassanzadeh *et al.* (2018)
ANZ IIP(4-VP/MMA)	30	4.365	Pb(II) Ni(II)	7.181 0.439	Neolaka *et al.* (2018)
Magnetic multiwall carbon nanotubes (MMWCNTs) IIP(4-VP/HEMA)	30	56.1	Cu(II) Ni(II)	12.32 16.39	Taghizadeh & Hassanpour (2017)
MPS-modified SBA-15 IIP(4-VP/MAA)	70	96.32	Cr(III) Cu(II) Cd(II) Ni(II)	15.00 9.63 16.67 12.50	This study

adsorption behavior of Cr(VI)-IIP was consistent with the Langmuir isotherm model and the PSO model, which indicated that the adsorption process for Cr(VI) tended to monolayer adsorption and was a chemical adsorption process. In addition, in the selective adsorption experiments, Cr(VI)-IIP showed a strong selective adsorption ability for Cr(VI) in the presence of competing ions such as Cr(III), Cu(II), Cd(II) and Ni(II), which demonstrated that Cr(VI)-IIP could be applied in complex aqueous environments to achieve efficient separation of Cr(VI), while enabling the separation of different valence states of elemental Cr. Finally, in the fixed-bed experiment, Cr(VI)-IIP showed ideal dynamic adsorption performance and high regeneration ability for Cr(VI), indicating that Cr(VI)-IIP possessed a fast adsorption rate and good stability. This study provided an efficient and novel method to precise identification and separation of Cr(VI), and the prepared Cr(VI)-IIP had enormous potential application in the preconcentration and separation of Cr(VI) from aqueous solution.

ACKNOWLEDGEMENTS

This work was financially supported by National Natural Science Foundation of China (No. 22178151) and Postgraduate Research Innovation Program of Jiangsu Province (No. SJCX22-1857).

DATA AVAILABILITY STATEMENT

All relevant data are included in the paper or its Supplementary Information.

CONFLICT OF INTEREST

The authors declare there is no conflict.

REFERENCES

Abu-Alsoud, G. F., Hawboldt, K. A. & Bottaro, C. S. 2020 Comparison of four adsorption isotherm models for characterizing molecular recognition of individual phenolic compounds in porous tailor-made molecularly imprinted polymer films. *ACS Applied Materials & Interfaces* **12** (10), 11998–12009.

Alahmad, W., Varanusupakul, P., Kaneta, T. & Varanusupakul, P. 2019 Chromium speciation using paper-based analytical devices by direct determination and with electromembrane microextraction. *Analytica Chimica Acta* **1085**, 98–106.

An, D.-Y., Pu, W.-R., Wang, Y., Xue, Z., Huang, Y.-P. & Liu, Z.-S. 2022 Improving sorption performance of a molecularly imprinted monolithic column by doping mesoporous molecular sieve SBA-15. *Microchimica Acta* **189** (3), 85.

Assi, N., Azar, P. A., Tehrani, M. S., Husain, S. W., Darwish, M. & Pourmand, S. 2019 Selective solid-phase extraction using 1,5-diphenylcarbazide-modified magnetic nanoparticles for speciation of Cr(VI) and Cr(III) in aqueous solutions. *International Journal of Environmental Science and Technology* **16** (8), 4739–4748.

Bagdat, S., Tokay, F., Demirci, S., Yilmaz, S. & Sahiner, N. 2023 Removal of Cd(II), Co(II), Cr(III), Ni(II), Pb(II) and Zn(II) ions from wastewater using polyethyleneimine (PEI) cryogels. *Journal of Environmental Management* **329**, 117002.

Bao, Y., Zhao, Y., Qin, G., Wang, J., Li, K. & Zhu, X. 2023 Histidine-mediated dendritic mesoporous magnetic ion-imprinted polymer toward effective and recoverable cadmium removal. *Colloids and Surfaces A: Physicochemical and Engineering Aspects* **656**, 130365.

Benhammou, A., Yaacoubi, A., Nibou, L. & Tanouti, B. 2007 Chromium(VI) adsorption from aqueous solution onto Moroccan Al-pillared and cationic surfactant stevensite. *Journal of Hazardous Materials* **140** (1–2), 104–109.

Biswas, A., Chandra, B. P. & Prathibha, C. 2023 Highly efficient and simultaneous remediation of heavy metal ions (Pb(II), Hg(II), As(V), As(III) and Cr(VI)) from water using Ce intercalated and ceria decorated titanate nanotubes. *Applied Surface Science* **612**, 155841.

Chen, S. Z., Wang, C. L., Yan, J. T. & Lu, D. B. 2020 Use of fibrous TiO_2@graphitic carbon nitride nanocomposites in dispersive micro-solid phase extraction for arsenic species before inductively coupled plasma mass spectrometry determination. *Microchemical Journal* **158**, 7.

Deng, S. B. & Bai, R. B. 2004 Removal of trivalent and hexavalent chromium with aminated polyacrylonitrile fibers: performance and mechanisms. *Water Research* **38** (9), 2424–2432.

Dobrzyńska, J., Dąbrowska, M., Olchowski, R., Zięba, E. & Dobrowolski, R. 2021 Development of a method for removal of platinum from hospital wastewater by novel ion-imprinted mesoporous organosilica. *Journal of Environmental Chemical Engineering* **9** (4), 105302.

Dolai, J., Ali, H. & Jana, N. R. 2019 Molecular imprinted poly-cyclodextrin for selective removal of dibutyl phthalate. *ACS Applied Polymer Materials* **2** (2), 691–698.

Ellerbrock, R., Stein, M. & Schaller, J. 2022 Comparing amorphous silica, short-range-ordered silicates and silicic acid species by FTIR. *Scientific Reports* **12** (1), 11708.

Faleschini, M., Giarratano, E. & Gil, M. N. 2023 Sorption of Cd(II), Cr(VI), Ni(II), and Pb(II) onto unmodified sludge from a pond treating woolen processing industry wastewater. *Water, Air, & Soil Pollution* **234** (3), 143.

Fallah, N. & Taghizadeh, M. 2020 Continuous fixed-bed adsorption of Mo(VI) from aqueous solutions by Mo(VI)-IIP: breakthrough curves analysis and mathematical modeling. *Journal of Environmental Chemical Engineering* **8** (5), 12.

Fang, L. L., Ding, L., Ren, W., Hu, H. Q., Huang, Y., Shao, P. H., Yang, L. M., Shi, H., Ren, Z., Han, K. K. & Luo, X. B. A. 2021 High exposure effect of the adsorption site significantly enhanced the adsorption capacity and removal rate: a case of adsorption of hexavalent chromium by quaternary ammonium polymers (QAPs). *Journal of Hazardous Materials* **416**, 11.

Fei, J. J., Wu, X. H., Sun, Y. L., Zhao, L. Y., Min, H., Cui, X. B., Chen, Y. J., Liu, S., Lian, H. Z. & Li, C. 2021 Preparation of a novel amino functionalized ion-imprinted hybrid monolithic column for the selective extraction of trace copper followed by ICP-MS detection. *Analytica Chimica Acta* **1162**, 10.

Ferreira, V. J., Lemos, V. A. & Teixeira, L. S. G. 2023 Dynamic reversed-phase liquid-liquid microextraction for the determination of Cd, Cr, Mn, and Ni in vegetable oils by energy dispersive X-ray fluorescence spectrometry. *Journal of Food Composition and Analysis* **117**, 105098.

Giove, A., El Ouardi, Y., Sala, A., Ibrahim, F., Hietala, S., Sievanen, E., Branger, C. & Laatikainen, K. 2023 Highly selective recovery of Ni(II) in neutral and acidic media using a novel Ni(II)-ion imprinted polymer. *Journal of Hazardous Materials* **444**, 130453.

Guo, W., Chen, R., Liu, Y., Meng, M., Meng, X., Hu, Z. & Song, Z. 2013 Preparation of ion-imprinted mesoporous silica SBA-15 functionalized with triglycine for selective adsorption of Co(II). *Colloids and Surfaces A: Physicochemical and Engineering Aspects* **436**, 693–703.

Hashami, Z. S., Taheri, A. & Alikarami, M. 2022 Synthesis of a magnetic SBA-15-NH_2@dual-template imprinted polymer for solid phase extraction and determination of Pb and Cd in vegetables; Box Behnken design. *Analytica Chimica Acta* **1204**, 339262.

Hassanzadeh, M., Ghaemy, M., Amininasab, S. M. & Shami, Z. 2018 An effective approach for fast selective separation of Cr(VI) from water by ion-imprinted polymer grafted on the electro-spun nanofibrous mat of functionalized polyacrylonitrile. *Reactive & Functional Polymers* **130**, 70–80.

Hua, S., Hu, Y., Zhao, L., Cao, L., Wang, X., Gao, J. & Xu, C. 2019 Selective removal of thiophene using surface molecularly imprinted polymers based on β-cyclodextrin porous carbon nanospheres and polycarboxylic acid functional monomers. *Energy & Fuels* **33** (12), 12637–12646.

Islam, A. & Rais, S. 2023 A facile approach for grafting ion imprinted polymer onto magnetic multi-walled carbon nanotubes for selective removal and preconcentration of cadmium in food and wastewater samples prior to atomic spectrometric determination. *Food Chemistry* **405**, 134751.

Jasim, A. N., Kamel, A., Al-Awadi, N. S. & Abd-Alrazack, H. F. 2023 Online column preconcentration for speciation and selective determination of Cr(III) in natural water samples using flow injection with chemiluminescence detection. *Luminescence* **38** (3), 360–368.

Kachbi, A., Arezoug, D., Kara-Abdelfettah, D., Benamor, M. & Senhadji-Kebiche, O. 2022 Determination of metal contents in aromatic herbs and spices from Algeria: chemometric approach. *Journal of Chemometrics* **36** (9), 1–12.

Kong, Z. Y., Du, Y. J., Wei, J. F., Zhang, H. & Fan, L. W. 2021 Synthesis of a new ion-imprinted polymer for selective Cr(VI) adsorption from aqueous solutions effectively and rapidly. *Journal of Colloid and Interface Science* **588**, 749–760.

Li, Z. C., Fan, H. T., Zhang, Y., Chen, M. X., Yu, Z. Y., Cao, X. Q. & Sun, T. 2011 Cd(II)-imprinted polymer sorbents prepared by combination of surface imprinting technique with hydrothermal assisted sol-gel process for selective removal of cadmium(II) from aqueous solution. *Chemical Engineering Journal* **171** (2), 703–710.

Li, G. B., Li, J. C., Zhang, S., Hou, X. S., Liu, X., Yu, Q. C. & Li, M. 2022 In-situ growing of metal-organic frameworks on iron mesh as a recyclable remediation material for removing hexavalent chromium from groundwater. *Chemosphere* **303**, 9.

Li, M., Kuang, S., Dong, J., Ma, H. & Kang, Y. 2023a Performance and mechanisms of Cr(VI) removal by nano-MnO_2 with different lattices. *Journal of Molecular Structure* **1275**, 134624.

Li, X., Liu, J., Feng, J., Wei, T., Zhou, Z., Ma, J., Ren, Y. & Shen, Y. 2023b High-ratio 100 plane-exposed ZnO nanosheets with dual-active centers for simultaneous photocatalytic Cr(VI) reduction and Cr(III) adsorption from water. *Journal of Hazardous Materials* **445**, 130400.

Li, X., Shi, Z., Zhang, J., Gan, T. & Xiao, Z. 2023c Aqueous Cr (VI) removal performance of an invasive plant-derived biochar modified by Mg/Al-layered double hydroxides. *Colloid and Interface Science Communications* **53**, 100700.

Li, Z., Yang, C., Qu, G., Cui, Q., Yang, Y., Ren, Y., Yang, Y. & Wang, F. 2023d Chitosan-modified magnetic carbon nanomaterials with high efficiency, controlled motility, and reusability-for removal of chromium ions from real wastewater. *Environmental Science and Pollution Research* **30**, 51271–51287.

Lin, C., Qiu, Y., Fan, J., Wang, M., Ye, L., Liu, Y., Ye, X., Huang, X., Lv, Y. & Liu, M. 2020 Fabrication of photo-responsive cellulose based intelligent imprinted material and selective adsorption on typical pesticide residue. *Chemical Engineering Journal* **394**, 124841.

Liu, Y., Meng, X. G., Han, J., Liu, Z. C., Meng, M. J., Wang, Y., Chen, R. & Tian, S. J. 2013 Speciation, adsorption and determination of chromium(III) and chromium(VI) on a mesoporous surface imprinted polymer adsorbent by combining inductively coupled plasma atomic emission spectrometry and UV spectrophotometry. *Journal of Separation Science* **36** (24), 3949–3957.

Liu, Y., Hu, X., Liu, Z., Meng, M., Pan, J., Jiang, Y., Ni, L. & Wu, W. 2017 A novel dual temperature responsive mesoporous imprinted polymer for Cd(II) adsorption and temperature switchable controlled separation and regeneration. *Chemical Engineering Journal* **328**, 11–24.

Liu, Z., Chen, L., Wang, Q., Yang, R., Hu, X., Liu, H., Li, J. & Liu, Y. 2022 Novel fluorescent recoverable probe based on carbon quantum dots/polypyrrole composite for the simultaneous determination of chromium(VI) and sulfite. *Journal of Molecular Structure* **1247**, 131409.

Luo, Z., Li, L., Guo, M., Jiang, H., Geng, W., Wei, W. & Lian, Z. 2020 Water-solid suspension grafting of dual monomers on polypropylene to prepare ion-imprinted fibers for selective adsorption of Cr(VI). *Fibers and Polymers* **21** (12), 2729–2739.

Mao, Y., Tao, Y., Zhang, X., Chu, Z., Zhang, X. & Huang, H. 2023 Removal of aqueous Cr(VI) by tea stalk biochar supported nanoscale zero-valent iron: performance and mechanism. *Water, Air, & Soil Pollution* **234** (3), 149.

Meng, M. J., Meng, X. G., Liu, Y., Liu, Z. C., Han, J., Wang, Y., Luo, M., Chen, R., Ni, L. & Yan, Y. S. 2014 An ion-imprinted functionalized SBA-15 adsorbent synthesized by surface imprinting technique via reversible addition-fragmentation chain transfer polymerization for selective removal of Ce(III) from aqueous solution. *Journal of Hazardous Materials* **278**, 134–143.

Mohana Rangan, S., Krajmalnik-Brown, R. & Delgado, A. G. 2021 An ion chromatography method for simultaneous quantification of chromate, arsenate, selenate, perchlorate, and other inorganic anions in environmental media. *Environmental Engineering Science* **38** (7), 626–634.

Moritz, M. & Laniecki, M. 2012 SBA-15 mesoporous material modified with APTES as the carrier for 2-(3-benzoylphenyl)propionic acid. *Applied Surface Science* **258** (19), 7523–7529.

Nchoe, O. B., Klink, M. J., Mtunzi, F. M. & Pakade, V. E. 2020 Synthesis, characterization, and application of β-cyclodextrin-based ion-imprinted polymer for selective sequestration of Cr(VI) ions from aqueous media: kinetics and isotherm studies. *Journal of Molecular Liquids* **298**, 111991.

Neolaka, Y. A. B., Supriyanto, G. & Kusuma, H. S. 2018 Adsorption performance of Cr(VI)-imprinted poly(4-VP-co-MMA) supported on activated Indonesia (Ende-Flores) natural zeolite structure for Cr(VI) removal from aqueous solution. *Journal of Environmental Chemical Engineering* **6** (2), 3436–3443.

Perez-Quintanilla, D., Sanchez, A., del Hierro, I., Fajardo, M. & Sierra, I. 2007 Preparation, characterization, and Zn^{2+} adsorption behavior of chemically modified MCM-41 with 5-mercapto-1-methyltetrazole. *Journal of Colloid and Interface Science* **313** (2), 551–562.

Pluhacek, T., Pechancova, R., Milde, D. & Bettencourt da Silva, R. J. N. 2023 Bottom-up uncertainty evaluation of complex measurements from correlated performance data: determination of total Cr in yeast by ICP-MS after acid digestion. *Food chemistry* **404**, 134466.

Rajaram, R., Ganeshkumar, A. & Emmanuel Charles, P. 2023 Ecological risk assessment of metals in the Arctic environment with emphasis on Kongsfjorden Fjord and freshwater lakes of Ny-Alesund, Svalbard. *Chemosphere* **310**, 136737.

Ren, B. Q., Song, X. X., Zhao, L. Y., Jin, Y., Bai, S. S., Cui, C. W. & Wang, J. Y. 2022 Water-based Fe_3O_4 magnetic fluid-coated *Aspergillus niger* spores for treating liquid contaminated with Cr(VI). *Environmental Research* **212**, 10.

Sobrinho, R. A. L., Andrade, G. R. S., Costa, L. P., de Souza, M. J. B., de Souza, A. & Gimenez, I. F. 2019 Ordered micro-mesoporous carbon from palm oil cooking waste via nanocasting in HZSM-5/SBA-15 composite: preparation and adsorption studies. *Journal of Hazardous Materials* **362**, 53–61.

Sun, Q., Aguila, B., Perman, J., Ivanov, A. S., Bryantsev, V. S., Earl, L. D., Abney, C. W., Wojtas, L. & Ma, S. 2018 Bio-inspired nano-traps for uranium extraction from seawater and recovery from nuclear waste. *Nature Communications* **9** (1), 1644.

Taghizadeh, M. & Hassanpour, S. 2017 Selective adsorption of Cr(VI) ions from aqueous solutions using a Cr(VI)-imprinted polymer supported by magnetic multiwall carbon nanotubes. *Polymer* **132**, 1–11.

Wang, W., Weng, D. & Wu, X. 2012 Structure evolution and thermal stability of $La_2O_3^-$ doped mullite fibers via sol-gel method. *Journal of Rare Earths* **30** (2), 175–180.

Wang, L., Luo, Y., Li, H., Yu, D., Wang, Y., Wang, W. & Wu, M. 2020 Preparation and selective adsorption of surface-imprinted microspheres based on hyperbranched polyamide–functionalized sodium alginate for the removal of Sb(III). *Colloids and Surfaces A: Physicochemical and Engineering Aspects* **585**, 124106.

Wang, X., Cheng, H., Min, Y., Li, X., You, L. & Li, J. 2022 Fe_3O_4@m-ZrO_2@Ag ternary magnetic nanocomposites for sensitive SERS sensing and photocatalytic removal of Cr(VI) and organic dyes. *Composites Part B: Engineering* **239**, 109959.

Xu, H., Gao, Y., Tao, Q., Li, A., Liu, Z., Jiang, Y., Liu, H., Yang, R. & Liu, Y. 2021 Synthesizing a surface-imprinted polymer based on the nanoreactor SBA-15 for optimizing the adsorption of salicylic acid from aqueous solution by response surface methodology. *New Journal of Chemistry* **45** (14), 6192–6205.

Zeng, B., Xu, W., Khan, S. B., Wang, Y., Zhang, J., Yang, J., Su, X. & Lin, Z. 2021 Preparation of sludge biochar rich in carboxyl/hydroxyl groups by quenching process and its excellent adsorption performance for Cr(VI). *Chemosphere* **285**, 131439.

Zeng, B., Li, J., Xiong, C., Lin, G., Wang, W. & Wu, Z. 2022 High-performance Zn-based coordination polymers selectively adsorb mercury ions from aqueous solutions. *Journal of Cleaner Production* **337**, 130551.

Zhang, M. Y., Huang, R. F., Ma, X. G., Guo, L. H., Wang, Y. & Fan, Y. M. 2019 Selective fluorescence sensor based on ion-imprinted polymer-modified quantum dots for trace detection of Cr(VI) in aqueous solution. *Analytical and Bioanalytical Chemistry* **411** (27), 7165–7175.

Zhang, H., Ma, R., Yang, Y. H., Huang, L. L., Chen, N. C. & Xie, Q. L. 2022 Study of ion-imprinted adsorbent materials on diatom-based Cr (VI) surfaces. *Materials Letters* **308**, 4.

Zhang, Y., Xiong, Y., Xian, Q., He, X., Dan, H. & Ding, Y. 2023 Efficient adsorption and in situ solidification of cesium from aqueous solution using mesoporous MnO_2@SBA-15. *Annals of Nuclear Energy* **180**, 109509.

Zhao, D. Y., Feng, J. L., Huo, Q. S., Melosh, N., Fredrickson, G. H., Chmelka, B. F. & Stucky, G. D. 1998 Triblock copolymer syntheses of mesoporous silica with periodic 50 to 300 angstrom pores. *Science* **279**, 548–552.

Zheng, Z., Duan, X. & Tie, J. 2022 One-pot synthesis of a magnetic Zn/iron-based sludge/biochar composite for aqueous Cr(VI) adsorption. *Environmental Technology & Innovation* **28**, 102661.

Zhou, Z., Liu, X., Zhang, M., Jiao, J., Zhang, H., Du, J., Zhang, B. & Ren, Z. 2020 Preparation of highly efficient ion-imprinted polymers with Fe_3O_4 nanoparticles as carrier for removal of Cr(VI) from aqueous solution. *Science of the Total Environment* **699**, 134334.

Zhou, H. Y., Ma, M. Y., Zhao, Y. K., Baig, S. A., Hu, S. F., Ye, M. Y. & Wang, J. L. 2022 Integrated green complexing agent and biochar modified nano zero-valent iron for hexavalent chromium removal: a characterisation and performance study. *Science of the Total Environment* **834**, 10.

First received 17 September 2022; accepted in revised form 16 April 2023. Available online 27 April 2023